Plug actuation and active manipulation in closed monolithic fluidics using backpressure

N. Vourdas[1,3], G. Pashos[2], E. Rizos[3], G. Kokkoris[1,2], E. Tsampasis[3],

E. Klouvidaki[2], A.G. Boudouvis[2] and V.N. Stathopoulos[3]

[1]*Institute of Nanoscience & Nanotechnology, NCSR Demokritos, Athens 15310, Greece*

[2]*School of Chemical Engineering, National Technical University of Athens, Zografou Campus, Athens 15780, Greece*

[1]*General Department, National and Kapodistrian University of Athens, Psachna campus, 34400, Evia, Greece*

Abstract

We explore the mechanisms to actuate and manipulate liquid plugs in monolithic closed channel fluidics with porous hydrophobic walls. Applying a small pressure, as much as 10 mbar, from the rear side of the porous wall, hereafter backpressure, the inherently pinned plug is depinned and flows through

downwards the fluidic. The method is reversible in that by removing the backpressure the plug sticks back again to the fluidic. 3D numerical simulations with the volume of fluid method, presented here for the first time, show that the velocity of the plug can be manipulated by adjusting the backpressure. The movement of the plug results from deformation – displacement phases which are observed in the simulation and are corroborated by experimental results, recorded inside fluidics. A simplified model based on measurements of back and front contact angles under backpressure is developed.

1. Introduction

Commercialization of Lab-on-Chip (LoC) for Point-of-Care (PoC) diagnostics call for low-cost materials and manufacturing processes [1-3]. Even though soft lithography and pertinent practices based on planar technology enabled the development of complex microfluidics with numerous applications, still substantial manual labor work, clean room facilities, advanced and costly manufacturing processes etc are required. Recently, microfluidics prepared by additive manufacturing such as 3D-printing [4, 5], or high throughput tools such as injection molding [6] have attracted much attention. In these latter techniques, time-consuming deep plasma etching [7], or waste producing wet dissolution [8], or stringent sealing processes are circumvented. Starting from a CAD file, these techniques may deliver monolithic microfluidics with complex geometries, with difficult to compete cost, either for prototyping with 3D-printing or for mass production with injection molding.

A critical aspect in microfluidics prepared by such methods is the manipulation of the liquids inside the channels [9]. Use of syringe pumps deteriorates the portability potential and impose difficulties when e.g. differential flow rates are needed throughout the fluidic. Resorting to methodologies such as electrowetting, entails the fabrication of electrodes and complex structures, both of which reduce the disposability and most importantly require either planar technology, or manual labor work, thus

diminishing the advantageous characteristics of additive manufacturing or injection molding, described above.

Versatile active tools, compatible to the advantageous characteristics of microfluidics delivered with 3D-printing or injection molding are still rare. Fabrication of discrete elements [10] some of which acting as valves [11], incorporation of whole Teflon gates [12], solutions with moving parts [13, 14], or based on thermo-responsive polymers [15, 16] etc are among the solutions that have been proposed so far, some of which have already put in the market. Simple, gravity-induced flows may also be well applicable for continuous flows [17].

An alternative approach may be pursued by adjusting the wetting phenomena of the liquids and the surfaces implicated in the system [18-20]. Such phenomena are crucial for, and have been used in modulating pressure-driven flow [21, 22], in electroosmotic flow [7] and in passive valving [23, 24]. Methods adjusting such phenomena involve electricity [25, 26] and respective tools and have been widely used in manipulating liquids and plugs with much success [27-29]. These latter techniques are now being considered as the flagship for plug manipulation. Though highly effective, they involve fabrication of electrodes, and in some cases necessitate fine nanostructure [30], which add additional fabrication steps after 3D-printing or injection molding. Wetting phenomena are also strongly related to the presence, surface density and pressure of gas pockets at the liquid/solid interface [19, 31], and may well control the drag resistance inside fluidics [32].

In this direction we have recently developed a tool to manipulate the mobility of droplets on porous surfaces, tuning the pressure, hereafter backpressure, at the rear side of a hydrophobic surface on top of which the droplet has been positioned. Adjusting this backpressure triggers actuation of the inherently pinned droplet. We have presented applications of this tool in actuation and mobility manipulation in open surfaces [33, 34], and provided the actuation mechanism in 2d [35] and in 3d [36] calculations, in

valving of open-channel fluidics [37], in digital operations [38], and in mobility control after droplet impingement [39].

In this work we demonstrate this tool as a method for liquid plug manipulation in closed channel fluidics, without need for electrodes, temperature differences or foreign particles. In Fig. 1 we present the operational principle of our method. The fluidic architecture is depicted in Fig. 1(a). Such geometries may be easily produced by 3D-printing or injection molding. The liquid phase is introduced in the central closed-channel fluidic. The side channels act as the gas pipelines, through which the gas is fed and the backpressure is applied. The walls of the main channel are porous and hydrophobic, while the external face walls are gas-tight, and hence the gas feed is directed only inwards. In this study the fluidic has been prepared by extrusion of a ceramic paste. However, the same principle may be used in fluidics prepared by 3D-printing, conventional casting processes etc. The only prerequisite is for the fluidic channel to have open pores, i.e. to be gas permeable, and hydrophobic walls.

When the liquid plug is introduced in the central channel, pins on to the surface as seen in Fig. 1(b). In this state the fluidic acts as a valve in the *off* position. When gas is fed on the side channels, as demonstrated in Fig. 1(c), backpressure starts to increase at the solid/liquid interface, and gas pockets evolve as illustrated in the inset of Fig. 1(c). Backpressure incites a series of changes in the wetting state, some of which will be discussed later. The outcome is that the plug eventually slides downwards and flows through, as depicted in Fig. 1(d). In this state the fluidic acts as a valve in the *on* position. This transition from *off* to *on*, is active and reversible since by removing the gas feed, and hence decreasing the backpressure the plug pins back to the surface, it renders the surface sticky and switch the valve *off*. With this the plug is actively manipulated inside the closed channel fluidic only by using gas feed, with ultra-low pressure as will be presented later.
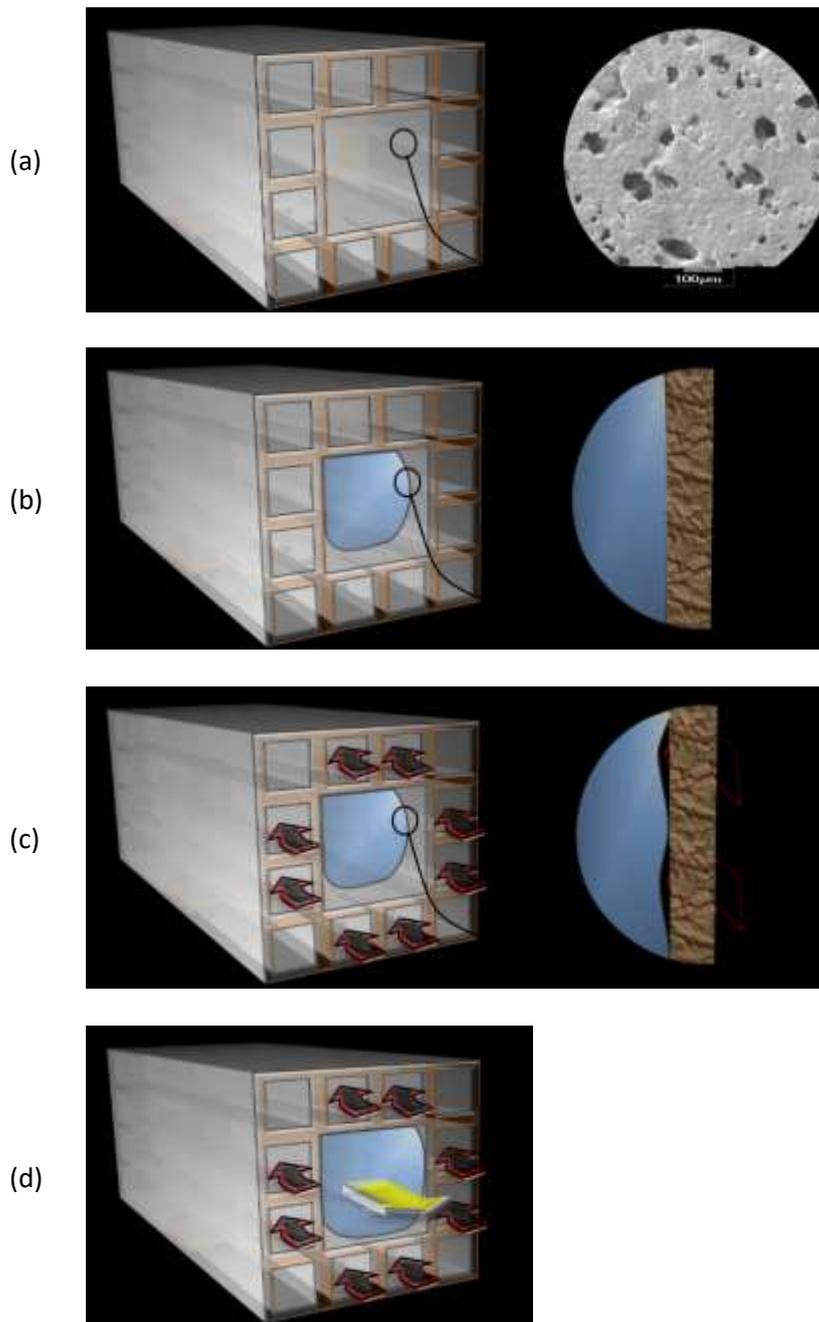
Fig. 1. Schematic illustration of the closed-channel valve operational principle. (a) The central channel will serve as the fluidic channel and will host the liquid plug. Through the side tubes the backpressure will be applied. The material is porous and hydrophobic, hence is gas permeable but not liquid permeable. The side faces have been sealed and are gas-tight. (b) A liquid plug is introduced in the central channel. The plug is sticky, and the valve is *off*. (c) Pressure is applied at the side channels, and gas pockets evolve. (d) The plug slides downwards and flows through. The valve is *on*.

2. Materials and Methods

Commercially available cordierite ($2MgO \cdot 2Al_2O_3 \cdot 5SiO_2$) was used for demonstration of our method. By proper machining, cutting and sealing, the desired architecture as seen in Fig. 1(a) was formed. In the inset of Fig. 1(a) a SEM image of the porous wall is depicted. The cordierite structure was rendered hydrophobic by immersion in a 0.5%wt Teflon solution (poly(4,5-difluoro-2,2-bis(trifluoromethyl)-1,3-dioxole-co-tetrafluoroethylene in Fluorinert FC-770) and then heated up to 110 ^{o}C for 20 min.

SL200 KS from Kino was used to measure the contact angles with an uncertainty of 2 mbar. The porous surface exhibits receding contact angle ca. 100° and advancing contact angle ca. 135°. Detailed sliding angle measurements for various droplet volumes and may be found in Ref. [33]. In the Results and Discussion (paragraph 3.3) the variations of the contact angles were measured *in situ* upon backpressure application, on a respective open surface, prepared exactly as the fluidic.

In all cases compressed air has been used for backpressure application. The pressure has been measured using the KIMO MP 200HP manometer with 2 mbar accuracy. No less than five measurements have been conducted for each case and pressures have been averaged.

3. Results and Discussion

3.1 Critical backpressure

In Fig. 2 we present the experimental results of the adequate backpressure values, hereafter critical backpressure, to actuate the plug, and hence to switch the valve to *on* position. Two different fluidics have been examined; one with cross-section of 1.5 mm x 1.5 mm in Fig. 2(a) and one with 0.8 mm x 0.8

mm in Fig. 2(b). The measurements depicted as 0deg correspond to a small tilt angle, less than 2 deg, since a small tilt angle is needed for the plugs to move directionally downwards.

For the 1.5 mm x 1.5 mm fluidic, backpressure as much as ca. 160 mbar is needed for plugs smaller than 10 uL. This pressure gradually reduces to values below 40 mbar for plugs bigger than 20 uL.

Backpressure values for the 0.8 mm x 0.8 mm fluidic are given in Fig. 2(b). Considerably lower values are needed in this case, with 12 mbar being the highest one. Moreover, the backpressure is virtually unaffected by the tilt angle and the droplet volume, considering that from 5 uL to 20 uL the backpressure varies at most from 12 to 7 mbar. This characteristic is rather advantageous and implies a high versatility of our method; to trigger the fluidic only one pressure is needed regardless the plug volume and the tilting. These backpressure values are close to the ones measured also for the open-channel fluidic [37].

(a)

(b)
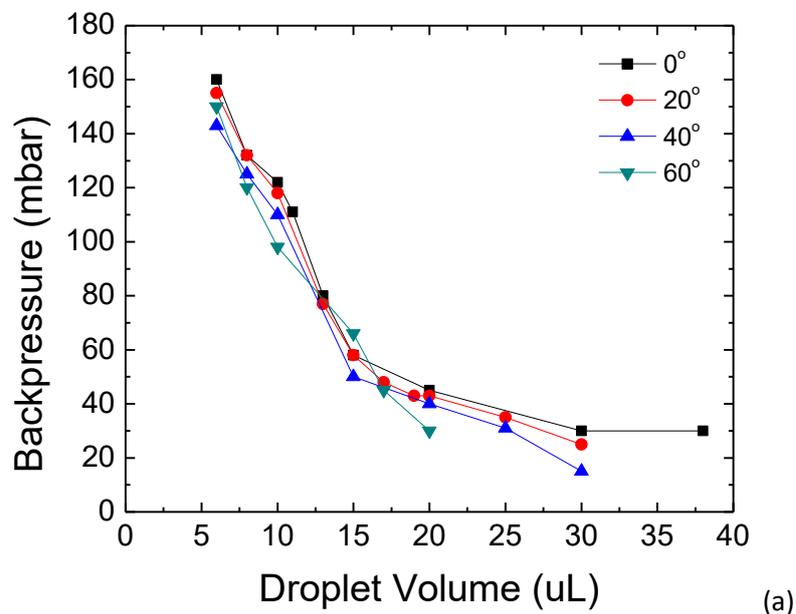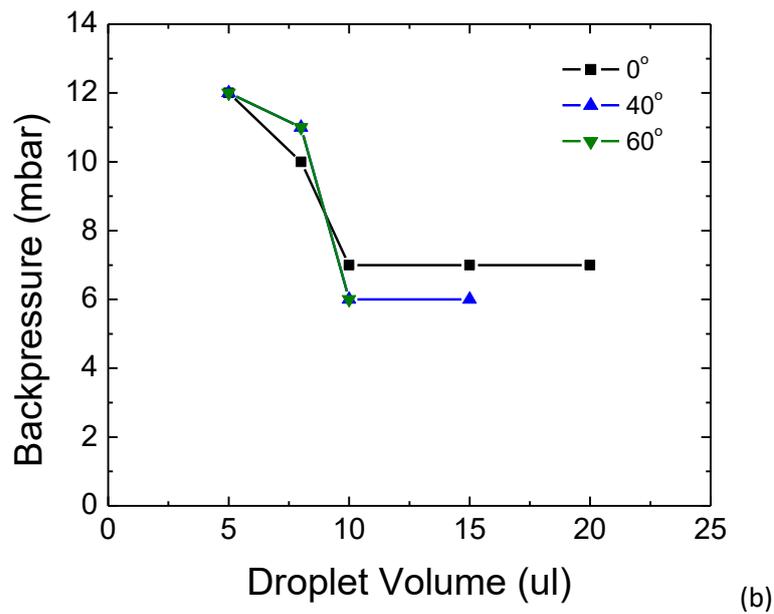
Fig. 2. Experimental measurements of the critical backpressure for actuation vs. droplet volume and tilt angle for fluidics with two cross sections: (a) 1.5 mm x 1.5 mm and (b) 0.8 mm x 0.8 mm. The backpressure exhibits an uncertainty of +/-2 mbar.

3.2 Numerical simulations and plug velocity manipulation

The travelling velocity of the plug can be manipulated by adjusting the backpressure, within an operating regime beyond its critical value. The increased gas flow rate causes strong perturbations leading to repeating and irregular movement of the liquid-gas interface that occurs in the vicinity of each pore, where gas 'attacks' the liquid. The cumulative effect of the localized perturbations incites the plug to an agitated state, where hysteresis effects are overcome, thus initiating downward movement (direction of gravity).

The liquid-gas interface in the closed channel fluidic can be easily visualized from the simulation results of a 3D square cross-section closed channel fluidic, revealing the agitated state of the plug (Fig. 3). However, experimental observation of the agitated state is impractical, whereas it can be easily performed in open channel fluidics and therefore, for that specific purpose, we have manufactured an

open channel fluidic. We argue that the purely qualitative comparison, presented in Fig. 3, between the open and closed channel fluidics is valid, because they share the fundamental mechanisms of plug movement. The developed numerical model is based on the volume of fluid (VOF) method including surface tension [40], applied to a small section (10 mm) of a vertical, closed fluidic with square cross-section (1.5 mm × 1.5 mm). Air permeates the fluidic at a constant rate, through uniformly pitched (300 um) pores with square cross-sections (50 um × 50 um). A 6.2 uL water plug is placed close to the upper end of the fluidic and under the combined effect of gravity and permeating air, the plug moves downwards.

The velocity of the plug is manipulated by adjusting the backpressure and consequently the flow rate of permeating air. The velocity of the plug increases with the flow rate of air, as it is seen from simultaneous snapshots from simulations of increasing flow rate in Fig. 4 – for an animation of the plug movement see the supplementary material. The fluidic containing a 6.2 uL water plug, exhibits normal operation for flow rates up to ~0.34 mL/s of air that permeates 10 mm of channel length. For higher values, the plug breaks up under the high stresses caused by air flow, which overcome the surface tension of water. In this event, air that gets trapped between the two halves of the plug, pushes them further apart, even against gravity (Fig. 4-- 0.38 mL/s, 0.61 mL/s).

When the backpressure is applied, starting from a resting position, the plug accelerates rapidly. The travelling velocity fluctuates around a mean value in an almost regular fashion as seen from the repeating patterns of the velocity-time plot in Fig. 6; the fluctuation can be attributed to the deformation – displacement phases observed during the movement of the plug (cf. Supplementary Material). The acceleration (the slope of the mean velocity in Fig. 6) decreases with time and it is expected that the velocity will reach a quasi-steady state at larger times. The fast response to changes in backpressure and the wide range of possible travelling velocities, contribute considerably to the advantages of the porous fluidics.
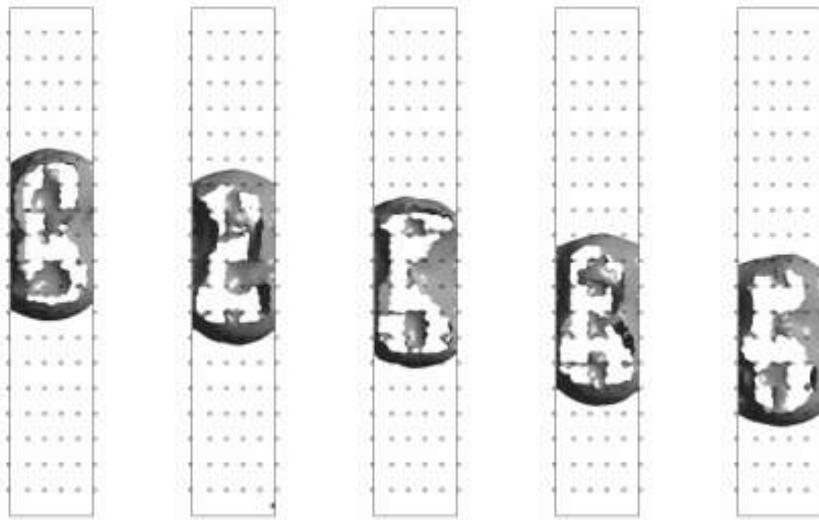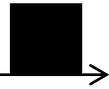
Fig. 3 Snapshots of a water plug (top-down view) during downward movement caused by the combined effect of gravity and permeating air. Upper row: snapshots from experiment in an open-channel fluidic with tilt angle (ca. 30°). Lower row: snapshots from simulation in a closed-channel vertical fluidic. The drawn shaded surface represents the air-liquid interface. The pores are depicted with the array of small rectangles on the surface of the fluidic.
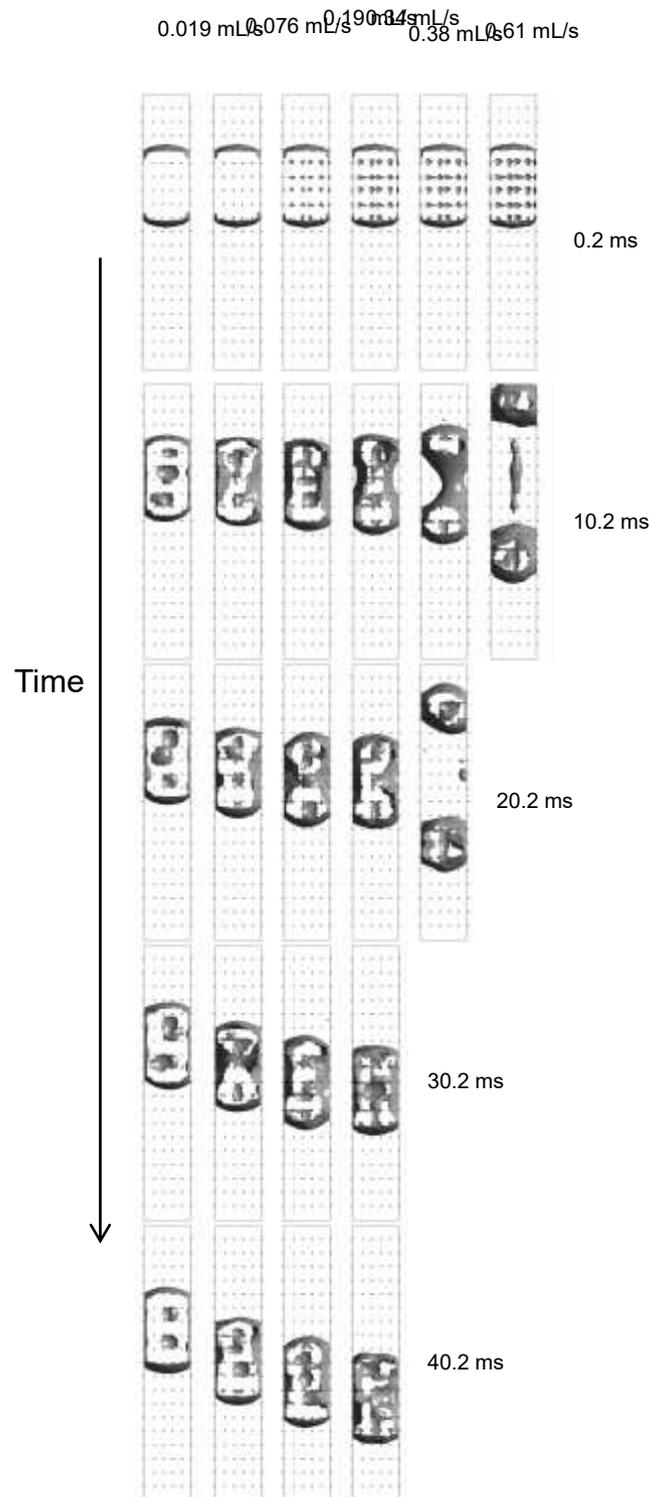
Fig. 4 Snapshots for 10 ms intervals (rows -- top to bottom) of six simulations with increasing values of air flow rate (columns -- left to right). The closed-channel fluidic is placed vertically and a 6.2 uL water plug moves downwards under the combined effect of gravity and permeating air, except for the two

highest flow rate simulations (two rightmost columns), where the plug breaks up and its halves move in opposite directions.

Similar behavior is also recorded experimentally as seen in Fig. 5. In Fig. 5a the plugs are in the start line, and in Fig. 5b a snapshots of the plugs is depicted after 0.5 s. In Fig. 5b the backpressure increases from 8, to 30, to 50 and to 80 mbar, from left to right. Backpressure controls the velocity of the plug, while at extreme backpressure values the plug may split into two.

(a)   (b)
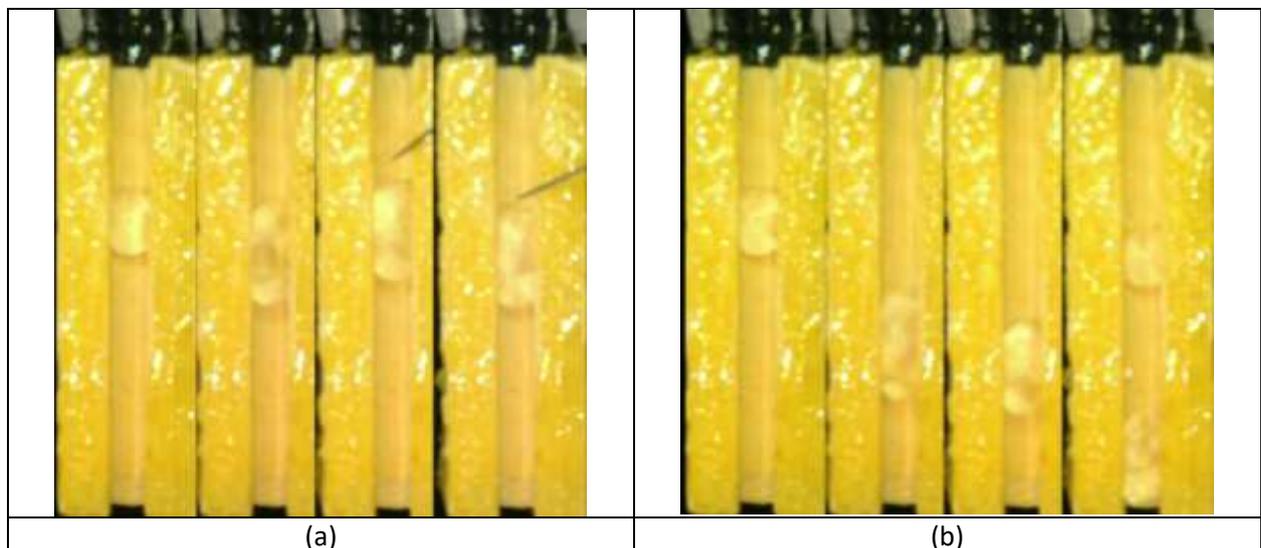
Fig. 5 Snapshots from the experimental behavior of a plug vs. backpressure. (a) Plugs before backpressure application, (b) Plugs after 0.5 s from backpressure application. The backpressure increases from left to right (8, 30, 50 and 80 mbar) yielding to the control of the plug velocity. For high backpressure values, as shown in the fluidic in the right.
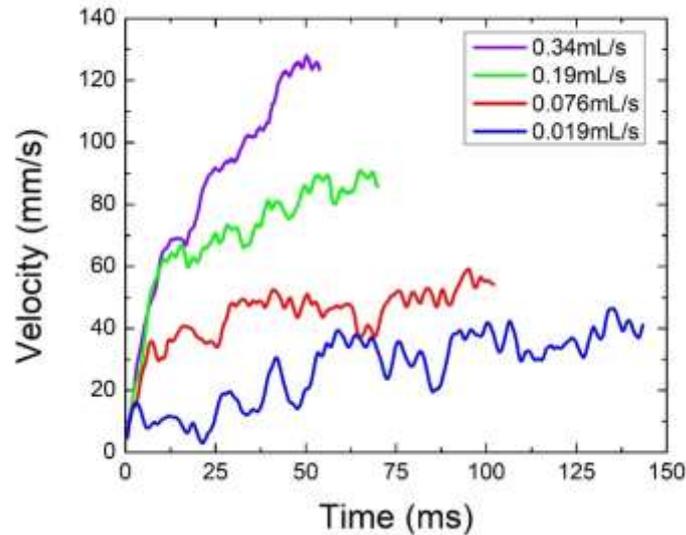
Fig. 6 Traveling velocity of a 6.2 uL water plug versus time for different air flow rates. Each plot line terminates when the plug reaches the outlet of the fluidic. For 0.34 mL/s the plug does not attain a quasi-steady velocity, because it continues to accelerate throughout the entire length of the fluidic. The application of high air flow rates (beyond 0.34 mL/s), causes consistently the break-up of the plug and therefore the traveling velocity has not been calculated.

3.3 Pressure balance –Analytical approach

As shown above, backpressure induces manifold variation to the plug and entail complex mechanisms; gas pockets evolve, new interfaces are formed and additional Laplace forces appear, shape deformations take place, liquid/solid surface area changes etc. Also transition from one wetting state to another on a rough surface require overcoming of energy barriers that cannot be easily followed analytically [41]. Based on the findings of section 3.2 the mechanisms of plug travelling beyond the critical backpressure cannot be followed analytically. However, the onset of movement may be understood analytically, by means of a simple model, accounting for the main pressures exerted on a plug moving inside a channel.

The pressure difference along a plug inside the fluidic is the following [42]:

$$\Delta P = P_r - P_a = \Delta P_c + \Delta P_h + \Delta P_e \qquad\qquad Eq.1$$

with ΔP_c is the difference in the capillary pressures, arising from the Laplace pressure at the two menisci, ΔP_h being the pressure evolved due to the gravitational forces, and ΔP_e being the external pressure difference at the receding and the advancing side. In our case and within this study ΔP_e is equal to zero. ΔP_c and ΔP_h are given by the following equations:

$$\Delta P_c = P_{c,front} - P_{c,back} = G\left[\left(\frac{\sigma cos\theta}{d}\right)_{front} - \left(\frac{\sigma cos\theta}{d}\right)_{back}\right] = G\frac{\sigma}{d}\left[\cos(\theta_{front}) - \cos(\theta_{back})\right] \quad Eq.2$$

$$\Delta P_h = \rho g L sin\varphi \qquad\qquad Eq.3$$

with d being the fluidic height, σ being the fluid surface tension (ca. 72 mN/m for the water), ρ being the fluid density (1 g/ml for the water), L being the plug length (see Fig. 7a), φ being the tilt angle (see Fig. 7), and G is constant specific to the channel geometry, equal to 4 for the case of a fluidic with square cross section.

The plug will begin to move when ΔP in Eq.1 becomes marginally positive. The parameters affected by the backpressure in *Eq.1* are: the front face (θ_{front}) and the back face (θ_{back}) contact angle, changing to θ^*_{front} and θ^*_{back}, respectively, as may be seen in Fig. 7. Similar behavior has been reported also for the case of drops transformed from a continuous flow [43].
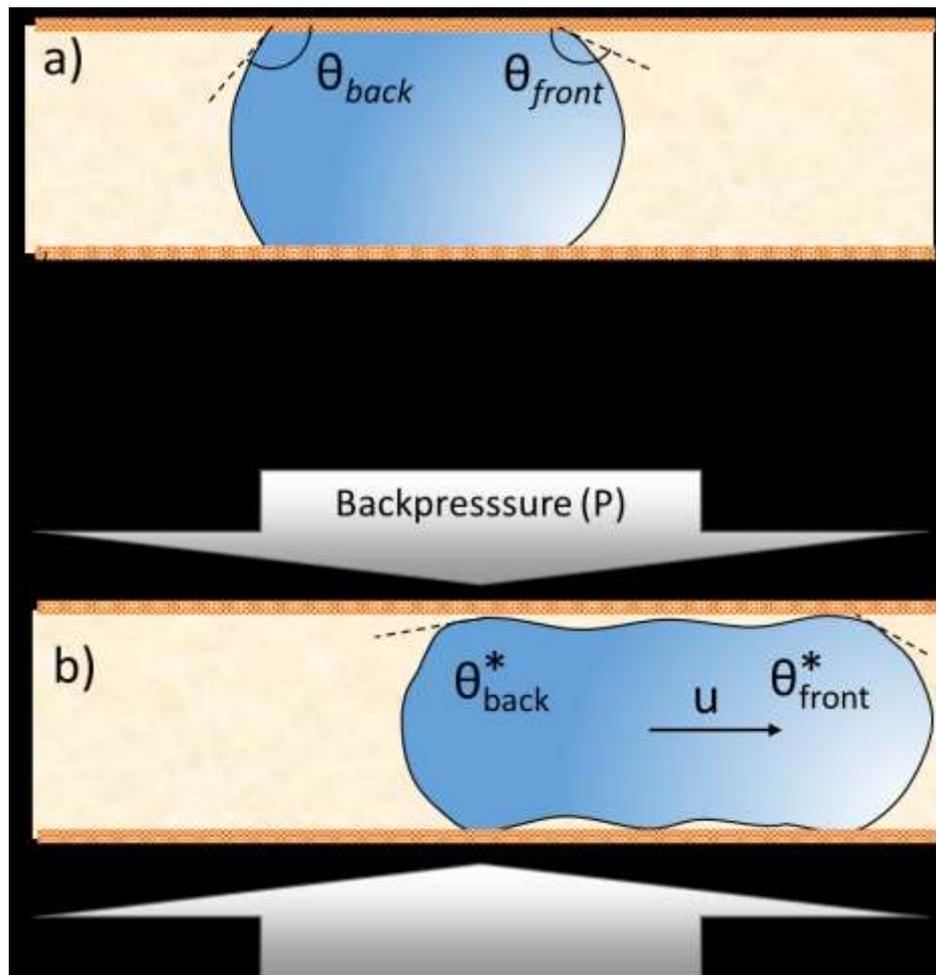
Fig. 7. Schematic representation of the mechanism for the actuation of a plug by means of backpressure. (a) The plug is pinned inside the fluidic. (b) Backpressure is applied though the porous hydrophobic walls, gas pockets evolve, and the plug is deformed. This is accompanied with a variation of θ_{front} and θ_{back}, to θ^*_{back} and θ^*_{front}, respectively.

This latter variation of θ_{back} and θ_{front}, to θ^*_{back} and θ^*_{front}, respectively, cannot be monitored *in* situ in the closed cordierite structure. For this reason, we followed the shape evolution of sessile droplets, resting and actuated on similar open porous surface upon backpressure application. In Fig. 8 we present snapshots and the measured CA variations from a 10 uL droplet on an open porous surface as surface tilted at different angles 20º and 40º.
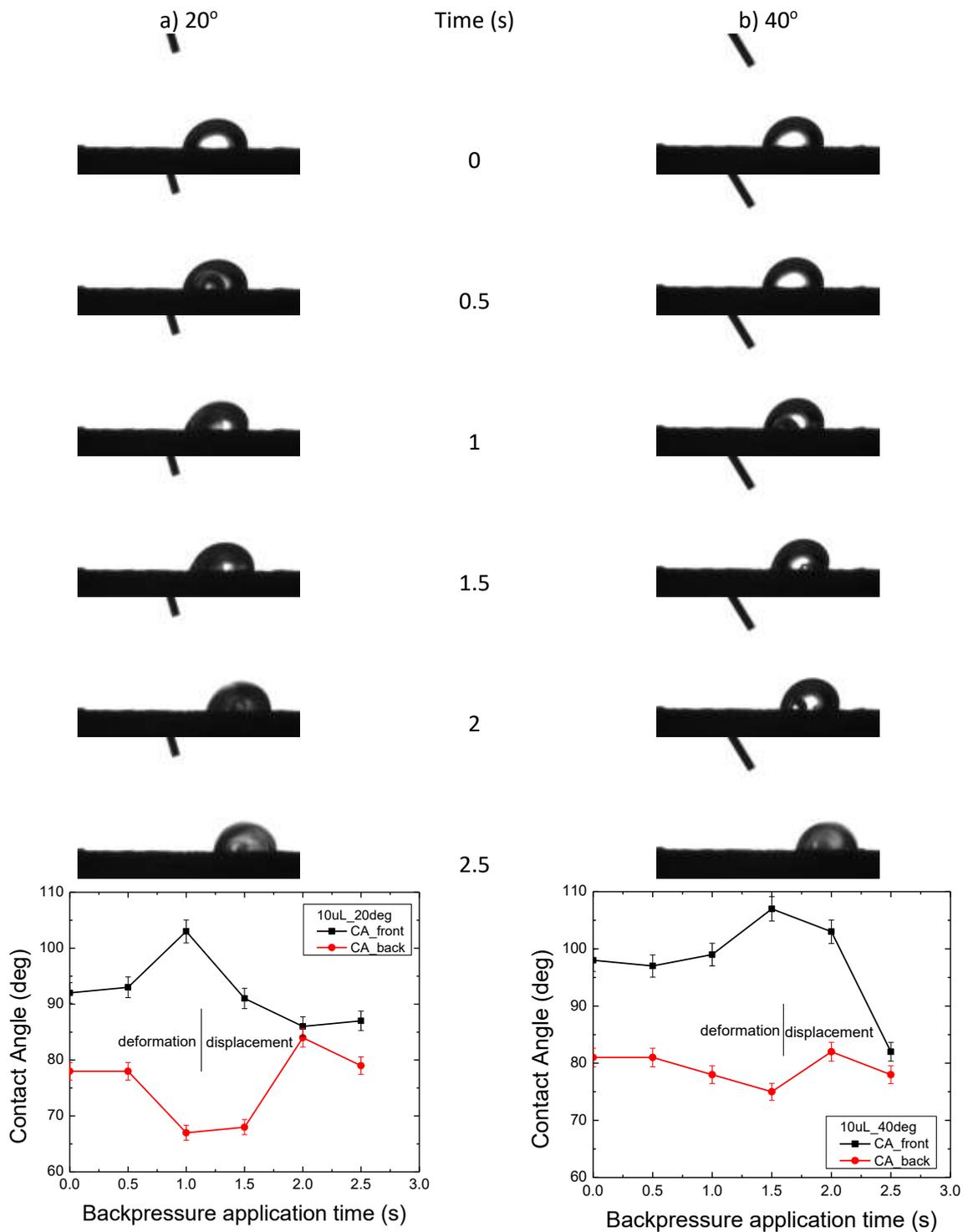
Fig. 8. Front and back face contact angle of a 10 uL droplet upon backpressure application tilted at (a) 20°, (b) 40°.

In all cases the quiescent droplet undergoes a phase of deformation upon backpressure application, during which the CA at the front and the back-phase change. This experimental observation is in line with the simulation presented in section 3.2. During displacement the difference between θ_{front} and θ_{back} minimizes. For example, and for a 10 uL droplet tilted at 20° θ_{front} is initially ca 92° and increases to ca. 104° after backpressure application, and after ca. 1 s. At 1.5s only the front face has been moved downwards. During the same time θ_{back} decreases from ca. 78° to ca. 66°. After this deformation the droplet undergoes a displacement during which θ_{front} - θ_{back} decreases to less than 2° as ca. 2 s; at this time the back face displaces also, while the droplet moves downwards. This cycle is repeated, namely the droplet deforms again, and then goes through a maximum θ_{front} followed by a displacement. This behavior is in accordance with the simulation results presented below.

These variations of θ_{front} and θ_{back} affect the ΔP_c exerted on the plug as seen from *Eq.2*. ΔP_c and ΔP_h have been calculated using the data from Fig. 8 and are demonstrated in Fig. 9 for the case of (a) 20°and (b) 40° tilt angle. In Fig. 9 - ΔP_c is plotted and compared to ΔP_h. In both cases the ΔP_h is initially smaller than $-\Delta P_c$. However, upon backpressure and the corresponding deformations, $-\Delta P_c$ becomes smaller resulting to plug displacement. For example, and for the 10uL plug tilted at 20°, ΔP_h becomes marginally bigger than $-\Delta P_c$ at ca. 2 s for both channel widths. At this point the pressure balance favors downward movement.

Backpressure is always higher compared to$-\Delta P_c$ and ΔP_h and therefore dominates over pressured evolved during deformation and displacement stages.
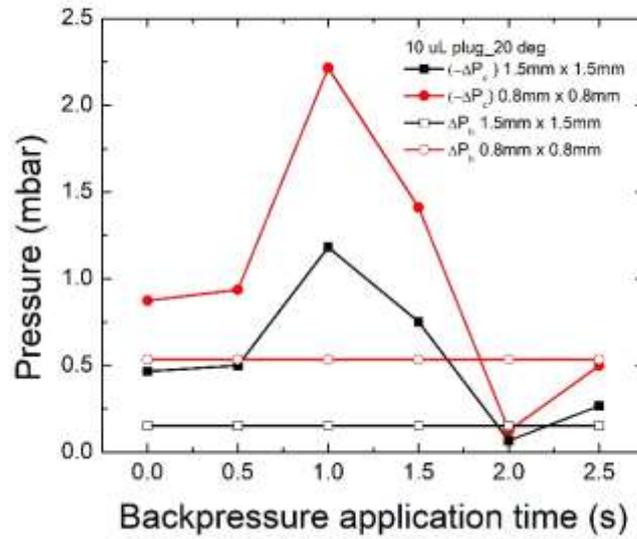
(a)
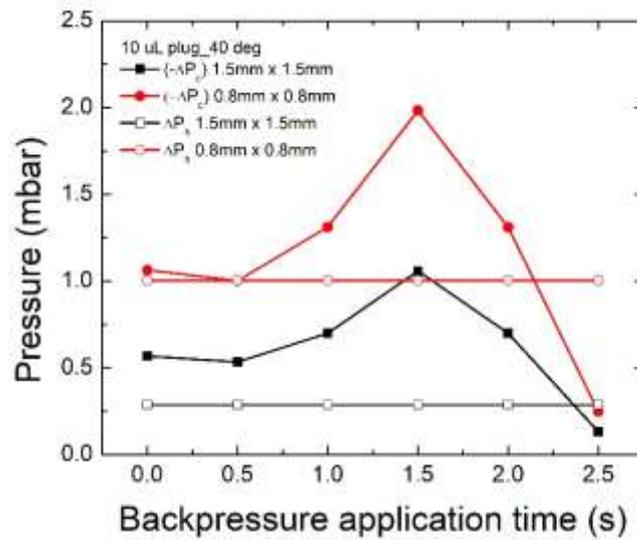
(b)

Fig. 9. Calculated values of ΔP$_c$ and ΔP$_h$ upon backpressure application of a 10 uL plug tilted at (a) 20° and (b) 40°. The backpressure exhibits an uncertainty of +/-2 mbar.

On the other hand, the gravitational pressure on the vertical axis, i.e. perpendicular to the porous surface, scales with channel height, H, as $P_h^\perp = \rho g H$. This yields a pressure less than 0.15 mbar in all cases studied herein. This pressure is negligible compared to the ones applied or evolved during movement and therefore is neglected. However, and because backpressure is applied from all surrounding surfaces the

plug is not fully levitated, as predicted numerically in paragraph 3.2 and monitored experimentally in this

(i.e. section 3.3) during the process, something that would require substantial energy inputs.

4. Conclusions

An alternative method for plug actuation and mobility manipulation in monolithic closed-channel fluidics

with porous hydrophobic walls has been demonstrated. By means of backpressure the initially pinned

plug depins and flows through downwards. Ultra-low backpressure values as much as 12 mbar are needed

to operate the device for fluidics with 0.8mm × 0.8mm cross section. The effect of backpressure has been

followed, by measuring the advancing and receding contact angle upon backpressure application, to

corroborate the numerical study. In all cases studied, the application of the backpressure results in droplet

deformation, and reduction of the hysteresis, thus leveraging the droplet movement. This mechanism has

been unveiled, here, both numerically and experimentally based on contact angle measurements during

backpressure application. This method provides a completely alternative means for plug manipulation

inside monolithic channels, without moving parts, circumventing the fabrication of electrodes, avoiding

introducing impurities in to the liquid phase, and ensuring thermal steadiness. It is amenable for

integration in monolithic metal, polymer or ceramic fluidics delivered by 3D-printing.

References

[1] G.M. Whitesides, The origins and the future of microfluidics, Nature, 442 (2006) 368-373.
[2] D. Moschou, N. Vourdas, G. Kokkoris, G. Papadakis, J. Parthenios, S. Chatzandroulis, A. Tserepi, All-plastic, low-power, disposable, continuous-flow PCR chip with integrated microheaters for rapid DNA amplification, Sensors and Actuators B: Chemical, 199 (2014) 470-478.

[3] M. Kitsara, J. Ducrée, Integration of functional materials and surface modification for polymeric microfluidic systems, Journal of Micromechanics and Microengineering, 23 (2013) 033001.

[4] A.K. Au, W. Huynh, L.F. Horowitz, A. Folch, 3D-Printed Microfluidics, Angewandte Chemie International Edition, 55 (2016) 3862-3881.

[5] C.M.B. Ho, S.H. Ng, K.H.H. Li, Y.-J. Yoon, 3D printed microfluidics for biological applications, Lab on a chip, 15 (2015) 3627-3637.

[6] C. Kokkinos, A. Economou, N.G. Goddard, P.R. Fielden, S.J. Baldock, Determination of Pb (II) by sequential injection/stripping analysis at all-plastic electrochemical fluidic cells with integrated composite electrodes, Talanta, 153 (2016) 170-176.

[7] N. Vourdas, A. Tserepi, A. Boudouvis, E. Gogolides, Plasma processing for polymeric microfluidics fabrication and surface modification: Effect of super-hydrophobic walls on electroosmotic flow, Microelectronic Engineering, 85 (2008) 1124-1127.

[8] M. Vlachopoulou, A. Tserepi, N. Vourdas, E. Gogolides, K. Misiakos, Patterning of thick polymeric substrates for the fabrication of microfluidic devices, Journal of Physics: Conference Series, 10 (2005) 293.

[9] J. Hereijgers, G. Desmet, T. Breugelmans, W. De Malsche, Strategies to integrate porous layers in microfluidic devices, Microelectronic Engineering, 132 (2015) 1-13.

[10] K.C. Bhargava, B. Thompson, N. Malmstadt, Discrete elements for 3D microfluidics, Proceedings of the National Academy of Sciences, 111 (2014) 15013-15018.

[11] J. Li, C. Liang, B. Zhang, C. Liu, A comblike time-valve used in capillary-driven microfluidic devices, Microelectronic Engineering, 173 (2017) 48-53.

[12] O. Cybulski, S. Jakiela, P. Garstecki, Whole Teflon valves for handling droplets, Lab on a chip, 16 (2016) 2198-2210.

[13] C.I. Rogers, K. Qaderi, A.T. Woolley, G.P. Nordin, 3D printed microfluidic devices with integrated valves, Biomicrofluidics, 9 (2015) 016501.

[14] A.K. Au, N. Bhattacharjee, L.F. Horowitz, T.C. Chang, A. Folch, 3D-printed microfluidic automation, Lab on a chip, 15 (2015) 1934-1941.

[15] C. Yu, S. Mutlu, P. Selvaganapathy, C.H. Mastrangelo, F. Svec, J.M.J. Fréchet, Flow Control Valves for Analytical Microfluidic Chips without Mechanical Parts Based on Thermally Responsive Monolithic Polymers, Analytical Chemistry, 75 (2003) 1958-1961.

[16] Q. Luo, S. Mutlu, Y.B. Gianchandani, F. Svec, J.M.J. Fréchet, Monolithic valves for microfluidic chips based on thermoresponsive polymer gels, Electrophoresis, 24 (2003) 3694-3702.

[17] P. Morier, C. Vollet, P.E. Michel, F. Reymond, J.S. Rossier, Gravity-induced convective flow in microfluidic systems: Electrochemical characterization and application to enzyme-linked immunosorbent assay tests, Electrophoresis, 25 (2004) 3761-3768.

[18] K. Tsougeni, N. Vourdas, A. Tserepi, E. Gogolides, C. Cardinaud, Mechanisms of oxygen plasma nanotexturing of organic polymer surfaces: from stable super hydrophilic to super hydrophobic surfaces, Langmuir, 25 (2009) 11748-11759.

[19] N. Vourdas, A. Tserepi, E. Gogolides, Nanotextured super-hydrophobic transparent poly (methyl methacrylate) surfaces using high-density plasma processing, Nanotechnology, 18 (2007) 125304.

[20] Y. Zhao, H. Wang, H. Zhou, T. Lin, Directional fluid transport in thin porous materials and its functional applications, Small, 13 (2017) 1601070.

[21] N.J. Shirtcliffe, G. McHale, M.I. Newton, Y. Zhang, Superhydrophobic Copper Tubes with Possible Flow Enhancement and Drag Reduction, ACS Applied Materials & Interfaces, 1 (2009) 1316-1323.

[22] M.N. Kavalenka, F. Vüllers, S. Lischker, C. Zeiger, A. Hopf, M. Röhrig, B.E. Rapp, M. Worgull, H. Hölscher, Bioinspired Air-Retaining Nanofur for Drag Reduction, ACS applied materials & interfaces, 7 (2015) 10651-10655.

[23] E. Gogolides, K. Ellinas, A. Tserepi, Hierarchical micro and nano structured, hydrophilic, superhydrophobic and superoleophobic surfaces incorporated in microfluidics, microarrays and lab on chip microsystems, Microelectronic Engineering, 132 (2015) 135-155.

[24] K. Tsougeni, D. Papageorgiou, A. Tserepi, E. Gogolides, "Smart" polymeric microfluidics fabricated by plasma processing: Controlled wetting, capillary filling and hydrophobic valving, Lab on a Chip - Miniaturisation for Chemistry and Biology, 10 (2010) 462-469.

[25] T.N. Krupenkin, J.A. Taylor, E.N. Wang, P. Kolodner, M. Hodes, T.R. Salamon, Reversible Wetting–Dewetting Transitions on Electrically Tunable Superhydrophobic Nanostructured Surfaces, Langmuir, 23 (2007) 9128-9133.

[26] A.G. Papathanasiou, Progress toward reversible electrowetting on geometrically patterned superhydrophobic surfaces, Current Opinion in Colloid & Interface Science, (2018).

[27] M. Abdelgawad, A.R. Wheeler, The Digital Revolution: A New Paradigm for Microfluidics, Advanced Materials, 21 (2009) 920-925.

[28] F. Mugele, J.-C. Baret, Electrowetting: from basics to applications, Journal of Physics: Condensed Matter, 17 (2005) R705.

[29] A. Milionis, C. Antonini, S. Jung, A. Nelson, T.M. Schutzius, D. Poulikakos, Contactless Transport and Mixing of Liquids on Self-Sustained Sublimating Coatings, Langmuir, 33 (2017) 1799-1809.

[30] N. Vourdas, D. Kontziampasis, G. Kokkoris, V. Constantoudis, A. Goodyear, A. Tserepi, M. Cooke, E. Gogolides, Plasma directed assembly and organization: bottom-up nanopatterning using top-down technology, Nanotechnology, 21 (2010) 085302.

[31] N.E. Vourdas, M.E. Vlachopoulou, A. Tserepi, E. Gogolides, Nano-textured polymer surfaces with controlled wetting and optical properties using plasma processing, International Journal of Nanotechnology, 6 (2009) 196-207.

[32] Y. Gao, J. Li, H.C. Shum, H. Chen, Drag Reduction by Bubble-Covered Surfaces Found in PDMS, Langmuir, 32 (2016) 4815–4819.

[33] N. Vourdas, C. Ranos, V.N. Stathopoulos, Reversible and dynamic transitions between sticky and slippery states on porous surfaces with ultra-low backpressure, RSC Advances, 5 (2015) 33666-33673.

[34] N. Vourdas, V.N. Stathopoulos, Droplet actuation and droplet mobility manipulation on porous surfaces by means of backpressure control, in: Technical Proceedings of the 2014 NSTI Nanotechnology Conference and Expo, NSTI-Nanotech 2014, 2014, pp. 220-223.

[35] N. Vourdas, G. Pashos, G. Kokkoris, A.G. Boudouvis, V.N. Stathopoulos, Droplet Mobility Manipulation on Porous Media Using Backpressure, Langmuir, 32 (2016) 5250–5258.

[36] P. Chrysinas, G. Pashos, N. Vourdas, G. Kokkoris, V.N. Stathopoulos, A.G. Boudouvis, Computational investigation of actuation mechanisms of droplets on porous air-permeable substrates, Soft matter, 14 (2018) 6090-6101.

[37] N. Vourdas, K. Dalamagkidis, V. Stathopoulos, Active porous valves for plug actuation and plug flow manipulation in open channel fluidics, RSC Advances, 5 (2015) 104594-104600.

[38] N. Vourdas, D.C. Moschou, K.A. Papadopoulos, D. Davazoglou, V.N. Stathopoulos, A new microfluidic pressure-controlled Field Effect Transistor (pFET) in digital fluidic switch operation mode, Microelectronic Engineering, 190 (2018) 28-32.

[39] N. Vourdas, A. Tserepi, V.N. Stathopoulos, Reversible pressure-induced switching of droplet mobility after impingement on porous surface media, Applied Physics Letters, 103 (2013) 111602.

[40] J.U. Brackbill, D.B. Kothe, C. Zemach, A continuum method for modeling surface tension, Journal of computational physics, 100 (1992) 335-354.

[41] G. Pashos, G. Kokkoris, A.G. Boudouvis, Minimum energy paths of wetting transitions on grooved surfaces, Langmuir, 31 (2015) 3059-3068.

[42] T.S. Sammarco, M.A. Burns, Thermocapillary pumping of discrete drops in microfabricated analysis devices, AIChE Journal, 45 (1999) 350-366.

[43] K. Mayur, N. Tuck Wah, Drops transformed from a continuous flow on a superhydrophobic incline, Journal of Physics D: Applied Physics, 46 (2013) 345302.